Geophysical Research Letters

RESEARCH LETTER
10.1029/2023GL105708

Solar Irradiance Modulates the Asian Summer Monsoon—ENSO Relationship Over the Last Millennium

Xiaojing Du[1], Sylvia Dee[1], Jun Hu[2], and Kaustubh Thirumalai[3]

[1]Department of Earth, Environmental, and Planetary Sciences, Rice University, Houston, TX, USA, [2]College of Ocean and Earth Sciences, Xiamen University, Xiamen, China, [3]Department of Geosciences, University of Arizona, Tucson, AZ, USA

Key Points:

- Solar irradiance altered the El Niño-Southern Oscillation (ENSO) and Asian summer monsoon relationship during the past millennium
- High solar irradiance weakens (strengthens) the ENSO-East Asian (South Asian) summer monsoon correlation
- Solar irradiance modulates the ENSO-ASM teleconnection through changes in the Western Pacific Subtropical High and ENSO event amplitude

Supporting Information:

Supporting Information may be found in the online version of this article.

Correspondence to:

X. Du,
xiaojing_du@brown.edu

Citation:

Du, X., Dee, S., Hu, J., & Thirumalai, K. (2023). Solar irradiance modulates the Asian summer monsoon—ENSO relationship over the last millennium. *Geophysical Research Letters*, *50*, e2023GL105708. https://doi.org/10.1029/2023GL105708

Received 1 AUG 2023
Accepted 8 NOV 2023

Abstract The Asian summer monsoon (ASM) is teleconnected to the El Niño Southern Oscillation (ENSO), but this relationship is nonstationary and has shifted significantly in recent decades. Characterizing the drivers of such shifts is crucial for improving ASM prediction and extreme event preparedness. Paleoclimate records indicate a link between ASM strength and solar activity on multidecadal-to-centennial timescales, but 20th-century data are too short to test mechanisms. Here we evaluate how solar irradiance influences the ASM-ENSO relationship using last-millennium paleoclimate data assimilation reconstructions and model simulations. We find that high solar irradiance weakens the ENSO-East Asian summer monsoon (EASM) correlation, but strengthens the ENSO-South Asian summer monsoon (SASM) correlation. Solar irradiance likely influences the strength of the ENSO-EASM and ENSO-SASM teleconnections via changes in the Western Pacific Subtropical High and the amplitude of ENSO events, respectively. We suggest a need for considering solar activity in decadal ASM rainfall predictions under global warming scenarios.

Plain Language Summary The Asian summer monsoon (ASM) affects over one-third of the world's population, with significant environmental and economic impacts. The ASM is influenced by the El Niño Southern Oscillation (ENSO), but the ENSO-ASM relationship has undergone notable changes in recent decades. Understanding the drivers of these changes is essential for improving ASM prediction. Previous studies based on individual records of past climate change have indicated a connection between ASM strength and solar activity over long periods, but 20th-century instrumental data are too short to fully understand this link. In this study, we investigated the influence of solar activity on the ENSO-ASM relationship using past climate records and model simulations spanning the last 1,000 years. We find that high solar irradiance weakens the ENSO-East Asian summer monsoon relationship while strengthening the ENSO-South Asian summer monsoon relationship. Solar irradiance might impact the strength of the ENSO-ASM relationship by causing changes in the air pressure systems over the western Pacific and the intensity of ENSO events. These findings imply that solar activity, combined with global warming, will affect rainfall in the ASM region. It is crucial to consider solar activity in the long-term prediction of ASM rainfall as the climate continues to warm.

1. Introduction

The Asian summer monsoon (ASM) is one of the most energetic climatic phenomena on Earth, with far-reaching environmental, societal, and economic impacts influencing over a third of the world's population (Clift & Plumb, 2008). The ASM drives seasonal rainfall that supplies freshwater resources for agriculture, forestry, and industrial development, and causes damaging typhoons and floods (B. Wang et al., 2006). Despite its societal and climatic importance, seasonal-to-decadal prediction of the ASM is still challenging, partly due to uncertainties surrounding its relationship with El Niño Southern Oscillation (ENSO), the most influential mode of interannual climate variability on Earth (Fan et al., 2012).

On interannual timescales, changes in sea surface temperature (SST) anomalies related to ENSO modulate ASM behavior via teleconnections, altering atmospheric/oceanic wave propagation and moisture supply to the region primarily driven by shifts in the Walker Circulation (Krishnamurthy & Goswami, 2000; Rasmusson & Carpenter, 1983; B. Wang et al., 2003). During El Niño years, the eastward shift of the Pacific Walker circulation and consequently enhanced low-level convergence over the equatorial Indian Ocean produces subsidence over the Indian subcontinent via the local Hadley circulation, resulting in weakened South Asian summer monsoon (SASM) circulation (Goswami, 1998; Palmer et al., 1992). Meanwhile, cold SST anomalies and suppressed convection in the equatorial western Pacific lead to reduced summer monsoon rainfall over the East Asian region

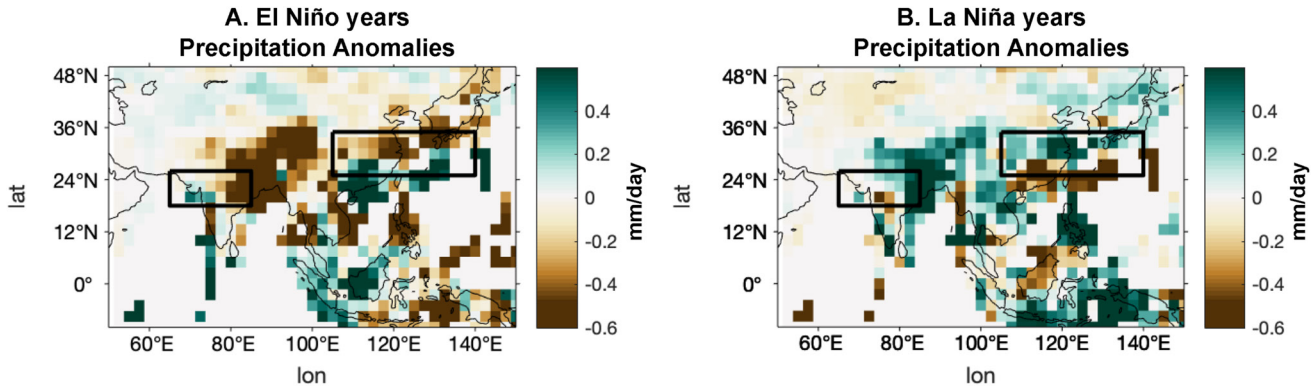

Figure 1. Composites of boreal summer (JJA) precipitation following (a) El Niño and (b) La Niña winters from 1901 to 2005 based on the Global Precipitation Climatology Centre data set (Schneider et al., 2011).

(B. Wang et al., 2000; R. Zhang et al., 1996). On average, this negative correlation between the ASM and ENSO is reflected in 20th-century observations based on the Global Precipitation Climatology Centre (GPCC) data set, which shows drier (wetter) conditions over northern India and central East Asia during the decay phase of El Niño (La Niña) events (Figure 1). However, this teleconnection between ENSO and the ASM is not consistent and exhibits substantial event-to-event variability, as well as multidecadal-scale fluctuations (Chen et al., 2022; Webster et al., 1998). For example, the negative relationship between the ASM and Niño 3.4 SST anomalies has apparently broken down since the late 1970s (Kumar et al., 1999; Wu & Wang, 2002).

Solar radiation is the primary source of energy driving atmospheric and oceanic circulation. Variations in total solar irradiance (TSI) are an important driver of climate system changes (Beer et al., 2000), including terrestrial climate (J. Wang et al., 2023). The coherence between ASM intensity and solar variability on multidecadal to centennial timescales has previously been recognized in paleoclimate records; accordingly, previous high-resolution paleoclimate studies have suggested TSI as one of the primary controls on Asian monsoon intensity (Neff et al., 2001; Tiwari et al., 2005; Y. Wang et al., 2005; J. Zhang et al., 2021). Oxygen isotope records from Dongge Cave suggest stronger EASM intensity corresponds to higher TSI over the Holocene (Y. Wang et al., 2005), whereas increased rainfall corresponding to weakened solar irradiance has been reported from mid-Yangtze River Valley (YRV) over the past two millennia (J. Zhang et al., 2021). In addition, lower precipitation over the Arabian Peninsula was reported during periods with low solar irradiance (Neff et al., 2001; Tiwari et al., 2005). However, it is still unclear how subtle changes in solar irradiance can significantly affect large-scale components of Earth's climate such as monsoon systems. Some work suggests that a small increase in solar irradiance can directly cause increased monsoon rainfall by strengthening the land-ocean thermal gradient and the monsoon winds, and/or by enhancing the evaporation and moisture flux from equatorial regions (Agnihotri et al., 2002; Mehta & Lau, 1997). In particular, modern observations suggest strong solar irradiance can enhance the ENSO-ASM relationship on multidecadal timescales by modulating the interaction of the monsoon systems and easterly trade winds over the tropical Pacific (Mehta & Lau, 1997). Other studies found that high solar activity can induce a northward expansion of the East Asian monsoon rain belt, leading to increased precipitation with larger variations across the Yangtze-Huaihe river basin (J. Wang & Zhao, 2012; Zhao & Wang, 2014; Zhao et al., 2017). Additionally, recent evidence suggests that solar irradiance can affect the mean state and variability of ENSO, which in turn amplifies the influence of solar irradiance through ENSO teleconnections (Emile-Geay et al., 2007; Narasimha & Bhattacharyya, 2010). This hypothesis is supported by instrumental records, which suggest increased solar irradiance weakens the Walker Circulation over the tropical Pacific via amplifying the Bjerknes ocean–atmosphere feedback (Misios et al., 2019), leading to an El Niño-like condition. Other studies suggest a weak La Niña-like response to solar maxima due to greater upwelling over the eastern tropical Pacific (Meehl et al., 2008; van Loon et al., 2007). Finally, recent work suggests that, due to variations of ocean heat content in the central Pacific Ocean, a La Niña-like pattern appears in the ascending phase of the solar cycle, whereas an El Niño-like pattern appears in the declining phase (Huo et al., 2022, 2023).

To date, limited literature has focused on how solar irradiance might influence the ENSO teleconnection to the ASM systems. Available evidence underscores the fact that a clear and comprehensive mechanism linking

fluctuations in solar irradiance to ASM impacts and its relationship with ENSO is still lacking (J. Zhang et al., 2021). Previous work has relied on one or a few paleoclimate records or on observations limited to the 20th century, which are too short to fully assess the influence of solar irradiance on the ENSO-ASM relationship over longer (e.g., decadal-to-centennial) timescales. To address these shortcomings, here we use the Community Earth System Model Last Millennium Ensemble (CESM-LME) (Otto-Bliesner et al., 2016) and two state-of-the-art paleoclimate data assimilation products: the Last Millennium Reanalysis (LMR, Hakim et al., 2016; Tardif et al., 2019a) and the Paleo Hydrodynamics Data Assimilation product (PHYDA, Steiger et al., 2018), to characterize the influence of solar irradiance on the ENSO-ASM relationship during the last millennium (LM hereafter). The CESM-LME provides a long-term model ensemble framework for understanding the relationship between ENSO and the ASM, and allows for evaluation of the relative contributions of different external forcings during the LM. As a complement to the CESM-LME, paleoclimate data assimilation (DA) techniques combine globally distributed paleoclimate proxy data with physical constraints of climate models to provide a spatially complete, dynamically consistent reconstruction of climate fields. We compare the response to solar irradiance in both paleoclimate DA products to climate model simulations from the LME. In doing so, we expand upon previous work by adding tens of thousands of years of additional realizations of climate and the ENSO-ASM relationship over several periods of high and low solar forcing. We focus our analyses on three key questions: (a) How does the ASM-ENSO teleconnection relationship (correlation) vary with time during the LM? (b) Does solar irradiance cause changes in the ASM-ENSO relationship? (c) If yes, what are the associated physical mechanisms?

2. Data and Methods

2.1. Climate Model and Paleoclimate Data Assimilation Products

2.1.1. CESM-LME

CESM-LME is an ensemble of simulations spanning the period of 850–2005 CE (Otto-Bliesner et al., 2016), forced with boundary conditions designed using estimates of the transient evolution of solar irradiance, volcanic emissions, greenhouse gasses, aerosols, land-use, and orbital forcing. The CESM-LME uses CESM v.1.1, with a resolution of ∼2° for the atmosphere and land models, and ∼1° for the ocean. Here, we analyze the output from the "full-forcing" ensemble members (including 13 simulations) containing all forcings mentioned above. Boreal summer (JJA) precipitation and winter (DJF) SSTs are used to characterize changes in the ASM and ENSO, respectively.

2.1.2. PHYDA

PHYDA is the first DA-based global reconstruction of hydroclimate and related dynamical variables spanning the last two millennia (Steiger et al., 2018). PHYDA integrates a network of 2,978 annually resolved proxy-data time series with CESM-LME climate simulations to reconstruct annually (April to the following March) and seasonally (JJA and DJF) resolved climate variables, including 2-m air temperature, the Palmer drought severity index (PDSI), and the standardized precipitation evapotranspiration index, on approximately a 2° latitude-longitude grid. Here, we use the JJA PDSI and DJF 2-m air temperature (as an approximation for SST) to evaluate the strength of the ASM and ENSO, respectively. As climate variables reconstructed by PHYDA do not include precipitation data, we use PDSI as an approximation for precipitation.

2.1.3. The LMR

LMR is a DA-based global climate reconstruction spanning the last two millennia (Hakim et al., 2016; Tardif et al., 2019a). LMR used the CCSM4 last-millennium climate simulation as its model prior and assimilated proxy data from the PAGES2k database (PAGES2k Consortium) to generate annually resolved (January-December) reconstructions of 2-m air temperature, SSTs, precipitation, PDSI, 500-hPa geopotential height, and sea level pressure (SLP) on a 2° latitude-longitude grid (Hakim et al., 2016). In this study, we analyzed LMR v2.0, which was designed to improve the reconstruction of hydroclimate variables by adding a large number of tree-ring records (Tardif et al., 2019a). Annual precipitation/PDSI and annual SST are used to characterize changes in ASM and ENSO, respectively.

2.2. Climate Index Definitions and Solar Irradiance Forcing

In this study, we use the Niño 3.4 index (the average of SST anomalies over 5°S–5°N, 170°–120°W) to characterize changes in ENSO (Trenberth, 1997). El Niño and La Niña events are defined when the Niño 3.4 index exceeds a threshold of 0.4°C. The Asian monsoon is usually divided into two subsystems because of their different

large-scale structures: the EASM and the SASM (Lau & Li, 1984; Tao, 1987). In this study, the EASM and SASM indices are defined as the average precipitation/PDSI anomalies across 25°–35°N, 105°–140°E (Takahashi & Fujinami, 2021), and 18°–26°N, 65°E–85°E (Saha et al., 2014), respectively. The solar forcing used in this study is based on the TSI reconstruction of Vieira, Solanki, Krivova, and Usoskin (Vieira et al., 2011), following CESM-LME (Otto-Bliesner et al., 2016). High/low TSI intervals are defined as periods with TSI values exceeding 0.5/falling below −0.5 standard deviations from the 850–1850 mean. The TSI time series was lowpass filtered with a 20-year cutoff to remove the 11-year Schwabe cycle and to highlight fluctuations of solar irradiance on multidecadal to centennial timescales. Note that when investigating the influence of TSI on the ASM-ENSO teleconnection during the past millennium, we restrict our analysis to 850–1850 for all data sets, including CESM-LME, PHYDA, and LMR, as well as index and TSI data, to purposefully exclude the anthropogenic influence of carbon emissions-induced hydroclimate trends.

3. Results

3.1. The ASM-ENSO Relationship Over the 20th Century and the Last Millennium

The composite analysis of the observational GPCC data set (spanning 1901–2005) suggests overall reduced EASM and SASM rainfall in response to El Niño events, and enhanced rainfall during La Niña events (Figure 1). During El Niño years, drier conditions spread throughout the ASM region with the exception of parts of the northwest coast of India, and southeast China between ∼15°N-24°N (Figure 1a). During La Niña (Figure 1b), the ASM region is wetter than average. The precipitation/PDSI anomalies in response to ENSO events between 1900 and 2000 in climate model simulations and DA products are generally consistent with modern observations (Figure S1 in Supporting Information S1), except for the EASM region in CESM-LME. Recent research (J. Hu et al., 2023) validated precipitation and PDSI derived from LMR and PHYDA against modern observations throughout the 20th century across the EASM and SASM regions, and concluded that both products exhibit fair agreement with instrumental data (J. Hu et al., 2023).

However, the ENSO-ASM teleconnection is nonstationary over the LM (Figure S2 in Supporting Information S1). Accordingly, we calculated 50-year moving correlations between Niño 3.4 and the East and South Asian monsoon indices from CESM-LME, LMR, and PHYDA (Figure S2 in Supporting Information S1) to characterize variations on multidecadal to centennial scales. As shown in Figure S2 of Supporting Information S1, the monsoon indices are generally negatively correlated with Niño 3.4 during 850–1850 CE, with mean correlation coefficient values (red solid line) below zero (black solid line); a notable exception is the EASM index correlation with Niño 3.4 in the CESM-LME (Figure S2a in Supporting Information S1). In addition, we identify several periods where the relationship between Niño 3.4 and the ASM index changes sign (marked by gray bars in Figure S2 of Supporting Information S1), yielding positive correlations between monsoon indices and Niño 3.4. This indicates that the negative correlation between ENSO and ASM, as seen in modern observations, experienced periods of breakdown over the last millennium.

3.2. The Impact of TSI on the ASM-ENSO Relationship

We further investigate the impact of TSI on the ASM-ENSO teleconnection by computing the composites of the precipitation/PDSI response to ENSO events during high and low TSI intervals. The average of precipitation/PDSI anomalies in all El Niño years between 850 and 1850 CE (regardless of TSI forcing) indicates widespread dry conditions over the EASM and SASM regions, extending to southeast China and the Maritime Continent (Figures 2a–2d), except for the EASM region in the CESM-LME (Figure 2a). The overall reduced ASM strength in response to El Niño events from 850 to 1850 is generally consistent with modern observations since 1901 (Figure 1).

Compared to average conditions, El Niño years during high TSI intervals tend toward wetter than usual conditions over the EASM region and drier than usual conditions in the SASM region (Figures 2e–2h). On the contrary, the EASM region tends to be drier than usual during El Niño years with low TSI (Figures 2i–2l), except for PDSI anomalies in PHYDA (Figure 2l). For the SASM region, wetter than usual conditions occur alongside low TSI forcing (Figures 2i–2k), except for PDSI anomalies in PHYDA (Figure 2l). In summary, our analysis reveals that during El Niño years when TSI is high, the EASM is significantly stronger (i.e., more rainfall, two-tailed *t*-test) compared to periods of low TSI; the SASM is significantly weaker when TSI is high (i.e., less rainfall, Figures 2m–2o). It is worth reiterating that no significant response was found in the PHYDA PDSI (Figure 2p). Considering that ASM

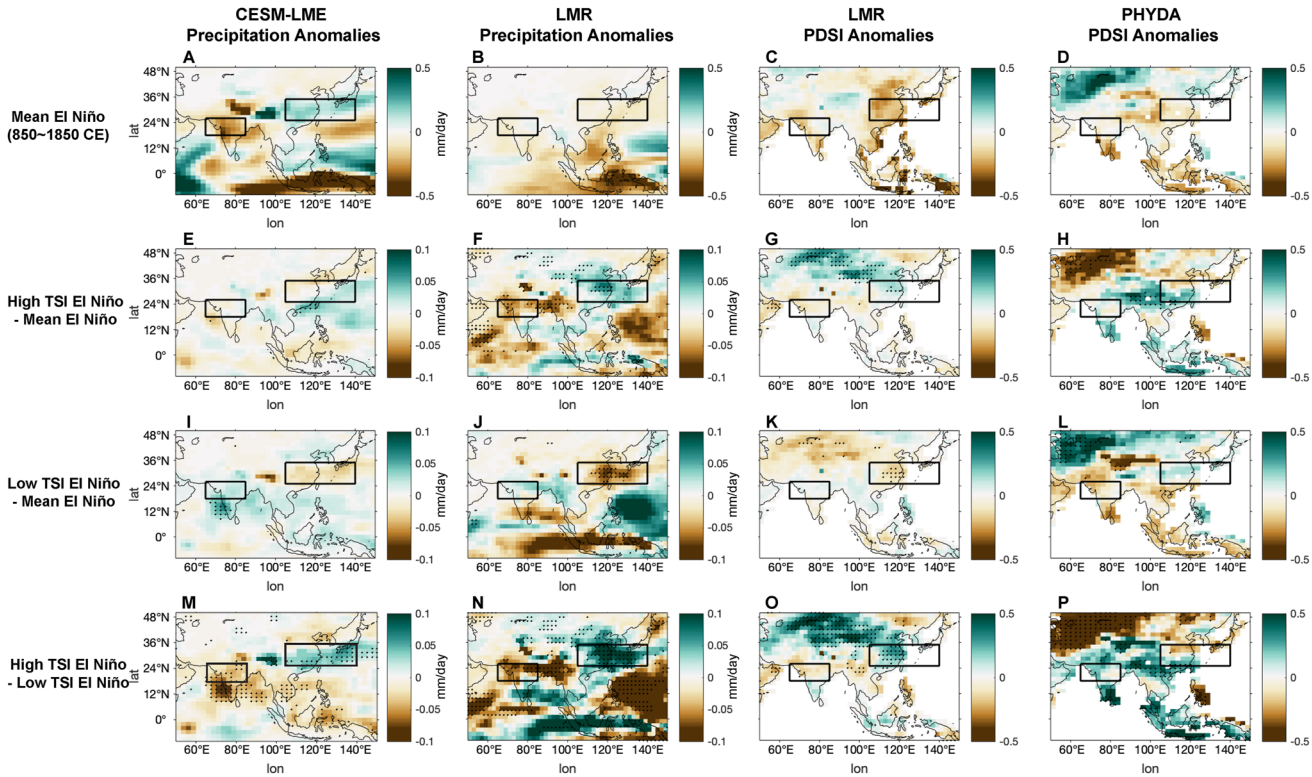

Figure 2. Hydroclimate response to El Niño events during high and low total solar irradiance (TSI) intervals. Panels (a–d) Average El Niño conditions from 850 to 1850 CE in (a) Community Earth System Model Last Millennium Ensemble JJA precipitation, (b) Last Millennium Reanalysis (LMR) annual precipitation, (c) LMR annual Palmer drought severity index (PDSI), and (d) Paleo Hydrodynamics Data Assimilation product (PHYDA) JJA PDSI. (e–h) Average precipitation/PDSI during El Niño years with high TSI minus average El Niño conditions from 850 to 1850 CE. Panels (i–l) are the same as (e–h), except that they are for low TSI intervals. (m–p) The difference between precipitation/PDSI of El Niño years during high TSI intervals and low TSI intervals. Stippling indicates regions passing the 95% confidence level of a two-tailed *t*-test. The number of samples included in each composite analysis is provided in Table S1 of Supporting Information S1.

intensity is reduced under usual conditions during El Niño years (Figures 1a and 2a–2d), these results suggest that high TSI weakens the EASM-ENSO teleconnection (less drying occurs during El Niño years), but strengthens the relationship between SASM and ENSO (drier than usual conditions during El Niño years). The influence of TSI on the ASM response during La Niña years is insignificant in both CESM-LME and PHYDA; furthermore, we observe inconsistent hydroclimate responses across the three data sets (Figure S3 in Supporting Information S1).

The impact of TSI on the ASM-ENSO relationship is also supported by changes in the correlation coefficient between ASM and Niño 3.4 indices. The EASM indices show a statistically significant weaker negative correlation with Niño 3.4 during high TSI intervals, suggesting a weakened EASM-ENSO teleconnection (upper panel in Figure 3, except for CESM-LME precipitation and LMR PDSI, which show a more positive correlation and insignificant change, respectively). In contrast, the relationship between the SASM and ENSO is stronger during high TSI intervals, as indicated by a more negative correlation between the SASM index and Niño 3.4 in all three data sets (Figures 3e–3h). To isolate the direct influence of TSI on the ASM, and to differentiate it from TSI's modulation of the ASM-ENSO relationship, we selected neutral ENSO years (with Niño 3.4 index between −0.4 and 0.4) during high and low TSI intervals, and calculated the precipitation/PDSI difference between the two periods (high TSI minus low TSI, Figure S4 in Supporting Information S1). The precipitation/PDSI anomalies during neutral ENSO conditions (Figures S4i–S4l in Supporting Information S1) are not statistically significant or are of a smaller magnitude compared to those in El Niño years (Figures 2m–2p), supporting the assertion that solar activity influences the strength of ASM via altering its teleconnection to ENSO.

3.3. Dynamics of the Large-Scale ENSO-ASM Teleconnection

To investigate the dynamics associated with the changes in the ENSO-ASM teleconnection response to TSI, we assessed the SST and SLP fields from LMR. PHYDA does not reconstruct dynamical fields and shows an

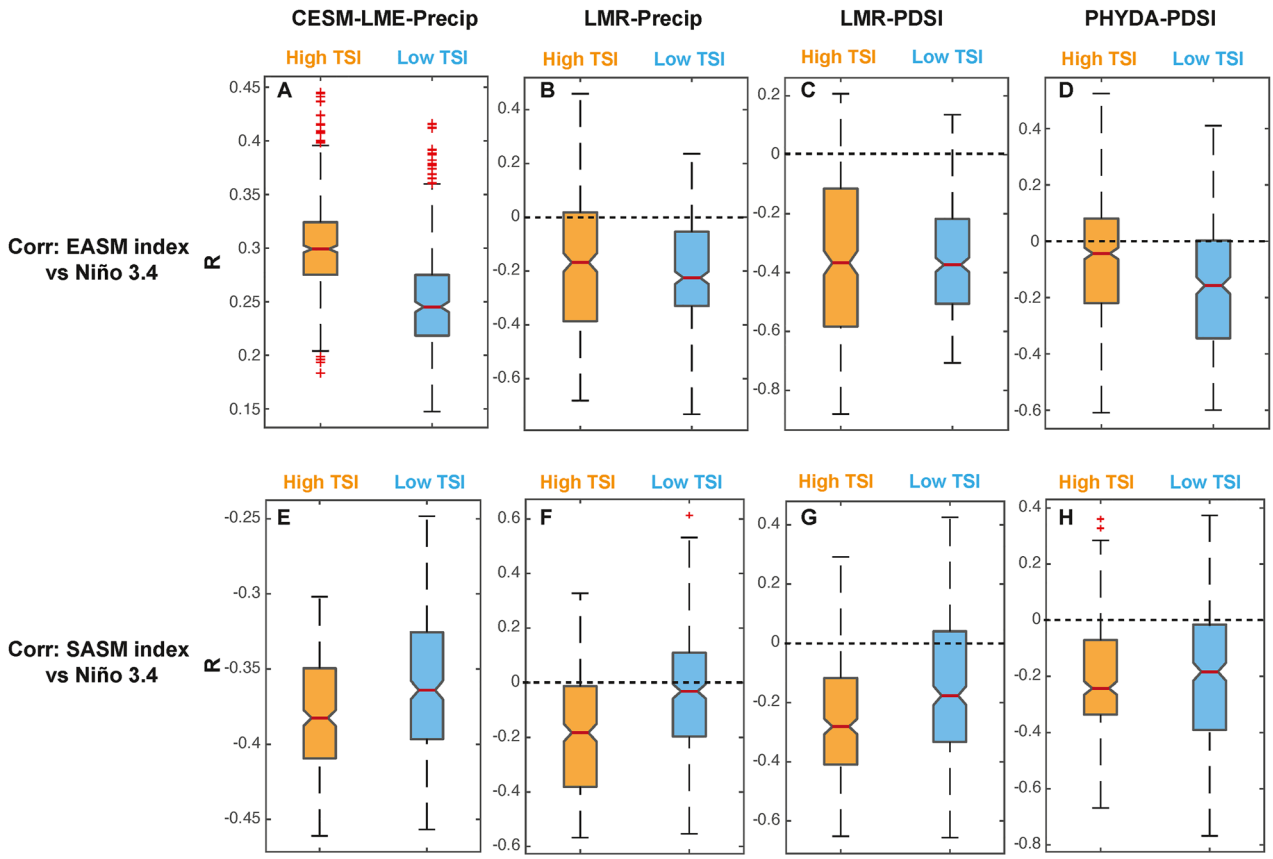

Figure 3. The correlation coefficient between Asian summer monsoon and Niño 3.4 indices during high and low total solar irradiance (TSI) intervals. Notched boxplots show the distribution of the correlation coefficients between the EASM index and Niño 3.4 index during high TSI (orange) and low TSI (blue) intervals in (a) Community Earth System Model Last Millennium Ensemble (CESM-LME) precipitation, (b) Last Millennium Reanalysis (LMR) precipitation, (c) LMR Palmer drought severity index (PDSI), and (d) Paleo Hydrodynamics Data Assimilation product (PHYDA) PDSI. Panels (e–h) same as (a–d), but with the correlation coefficients between South Asian summer monsoon and Niño 3.4 indices. The bottom, top, and red solid lines in the middle of each box represent the 25th, 75th, and the median percentiles of correlation coefficients. The notch width indicates the 95% confidence level of the median.

insignificant response to TSI in the composite analysis (Figure 2 and Figure S3 in Supporting Information S1). Additionally, CESM-LME does not capture the negative EASM-ENSO relationship found in instrumental observations (Figure 1). By contrast, recent research (J. Hu et al., 2023) demonstrates both annual precipitation and PDSI derived from LMR are consistent with modern 20th-century observations. Furthermore, during 850–1850 CE, the annual precipitation/PDSI anomalies over the ASM domain (Figures 2b and 2c) and large-scale SST anomalies (Figures S6c and S6d in Supporting Information S1) in response to ENSO events from the LMR are generally consistent with the boreal summer (JJA) data derived from PHYDA (Figure 2d; Figures S6e and S6f in Supporting Information S1) and CESM-LME (Figure 2a; Figures S6a and S6b in Supporting Information S1), except for the EASM precipitation from CESM-LME (Figure 2a). Therefore, we focus only on the LMR results in the discussion that follows.

The LMR shows that anomalously warmer SSTs together with lower SLP over the central and eastern tropical Pacific occur during El Niño years with high TSI, indicating stronger than normal El Niño conditions (Figures 4a and 4b). Anomalously warmer SSTs exist over the equatorial eastern Indian Ocean and the Indonesian archipelago, as well as over the South China Sea and the Bay of Bengal (Figure 4a). The Western Pacific Subtropical High (WPSH) strengthens and shifts westward during El Niño years with high TSI (Figure 4b). Additionally, the Aleutian Low deepens and expands over the North Pacific, accompanied by a broad low-pressure anomaly over the ASM region and the tropical Indian Ocean (Figure 4b).

During high TSI intervals, anomalously warm SSTs over the central and eastern tropical Pacific (Figure 4a) likely drive even drier conditions over northern India and thus a more negative (stronger) correlation between the

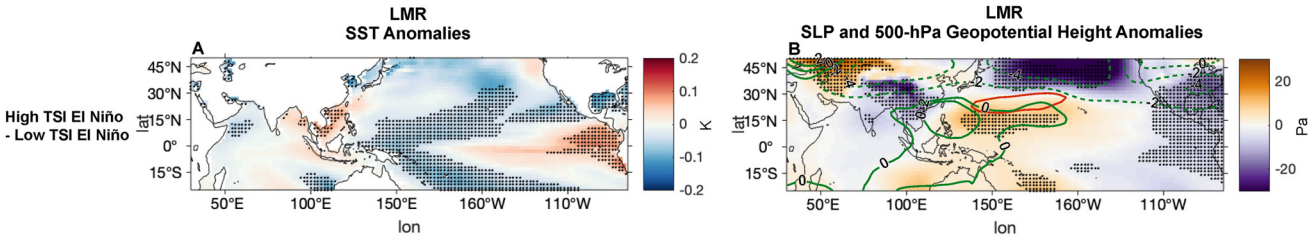

Figure 4. The difference between annual (a) sea surface temperature (SST) and (b) sea level pressure (SLP) and 500 hPa geopotential height (green contours) of El Niño years during high total solar irradiance (TSI) intervals and low TSI intervals in Last Millennium Reanalysis (LMR). The solid (dashed) green contours represent anomalously higher (lower) geopotential height. The solid red contour represents the climatological location of the Western Pacific Subtropical High, as indicated by the JJA mean of the 5,880 gpm (geopotential meters) geopotential height at 500 hPa from 1948 to 2022, based on the NCEP-NCAR Reanalysis 1 data (Kalnay et al., 1996). Stippling indicates regions passing the 90% confidence level of the *t*-test. The number of samples included in each composite analysis is provided in Table S1 of Supporting Information S1.

SASM and ENSO. The anomalous eastward movement of the Pacific Walker circulation during El Niño events appears to enhance precipitation over the equatorial Indian Ocean and produce subsidence and reduced monsoon rainfall over the Indian continent through the local Hadley circulation (Goswami, 1998; Goswami et al., 1999). When TSI is high, anomalously warm central and eastern tropical Pacific SSTs, or a stronger warm phase of ENSO, can, therefore, reinforce the anomalous Hadley circulation over the tropical Indian Ocean and the Indian continent, further weakening SASM circulation. Finally, we note that the SST anomalies in the tropical Pacific during periods of high TSI of LM are consistent with 20th-century observations and model simulations forced by solar irradiance variations. Taken together, this analysis of the LMR provides evidence showing that increased TSI warms the equatorial Pacific via surface heating. Previous studies suggest that on decadal to interdecadal timescales, this equatorial Pacific warming induced by high TSI would initiate a weaker east-west pressure gradient and reduce the Pacific Walker circulation, which would be further amplified by the Bjerknes feedback (Misios et al., 2019; White et al., 1997). This is akin to the SST and SLP anomalies during El Niño years in high TSI intervals observed from the LM (Figure 4).

The weakened EASM-ENSO relationship reconstructed during high TSI intervals is characterized by increased precipitation over the YRV during El Niño years. This could be associated with the westward intensification of the WPSH revealed by LMR SLP 500 hPa geopotential height anomalies (Figure 4b). The southerly wind of the western flank of the WPSH transports tropical moisture to East Asia (Lau & Li, 1984; Zhou & Yu, 2005). Therefore, the position and intensity of the WPSH both strongly influence the variability of EASM precipitation (Chang et al., 2000; Park et al., 2010; Zhou et al., 2009). A stronger and westward-shifted WPSH would intensify the Mei-Yu front, extend the duration of the front over the YRV, and enhance the supply of tropical moisture to eastern China (Chang et al., 2000). Barring other influences, these processes would typically contribute to a wetter EASM during high TSI intervals. We note previous studies based on instrumental records also reported increased precipitation in the EASM domain during high TSI years, partially due to the westward expansion of the WPSH (J. Wang & Zhao, 2012; Zhao & Wang, 2014; Zhao et al., 2017). Moreover, the observed increase in precipitation over the YRV since the late 1970s, along with the breakdown of the negative EASM-ENSO correlation, has been attributed to a westward shift of the WPSH (Z. Z. Hu, 1997; Yu & Zhou, 2007). Instrumental observations and climate model experiments have suggested the Indian Ocean-western Pacific warming and the Northwestern Pacific cooling contribute to an enhanced WPSH (B. Wang et al., 2013; Zhou et al., 2009), consistent with the SST anomalies reconstructed in LMR during El Niño years with high TSI (Figure 4a). Lin et al. (2021) found a similar pattern in the correlation between SST, SLP, and TSI in modern observations: warm SSTs over the Maritime Continent, central and eastern tropical Pacific, and cooling over the western North Pacific, along with intensified WPSH during solar active intervals. The authors attributed this pattern to upper tropospheric warming induced by solar heating and a weakened Hadley cell over the North Pacific. While such analysis is not possible with the limited fields afforded by LMR, the analyses from instrumental data support the linkage between TSI and the patterns of SST and SLP observed in LMR.

Furthermore, a stronger WPSH in response to high TSI is also observed during La Niña years, accompanied by warm SSTs over the Maritime Continent and cooling over the western North Pacific. This confirms the robust relationship between TSI, SST, and SLP. However, the intensified EASM in response to high TSI and strengthened WPSH is more pronounced during El Niño years (Figure S4b in Supporting Information S1) and less

pronounced during La Niña years (Figure S4f in Supporting Information S1). These distinct responses may be attributed to differences in the pressure systems over the ASM domain, as well as the Indian Ocean SST patterns during El Niño (Figure 4) and La Niña (Figure S5 in Supporting Information S1) years. The SST pattern differences may additionally involve intricate interactions between ENSO and the Indian Ocean Dipole, which are beyond the scope of this study.

4. Discussion and Conclusions

This study examined the influence of TSI on the evolution of the ENSO-ASM teleconnection over the LM using the CESM-LME and two paleoclimate DA reconstructions (LMR and PHYDA). We found the EASM and SASM indices are generally negatively correlated with Niño 3.4 over the LM (Figure S2 in Supporting Information S1), but exhibit large variations on multidecadal to centennial timescales, which we interpret as non-stationarity in the ASM-ENSO teleconnection. During high TSI intervals, the EASM-ENSO teleconnection is weakened: there is a less negative correlation between the EASM and Niño 3.4 indices, and increased monsoon rainfall during El Niño years (Figure 3). Drier than normal conditions are reconstructed for northern India along with more negative correlations between the SASM and Niño 3.4 indices, suggesting a stronger SASM-ENSO relationship. Therefore, our results suggest that solar irradiance influences the strength of EASM and SASM via modulation of ENSO teleconnections. To pinpoint the dynamics of how TSI affects ENSO and ultimately the ASM, we compared the changes in large-scale SST and SLP in response to El Niño years during high and low TSI in LRM. Stronger El Niño conditions characterized by anomalously warm central and eastern tropical Pacific SST intensify the SASM-ENSO correlation and enhance drying over the Indian continent. At the same time, the westward intensification of the WPSH leads to increased EASM rainfall and a weaker ENSO teleconnection to East Asia.

We found opposite responses to high TSI in the EASM and SASM subsystems, contrary to the anticipated in-phase intensification associated with an increased land-ocean heating gradient caused by direct radiative forcing. Additionally, the influence of solar irradiance alone (high TSI vs. low TSI in neutral-ENSO conditions) is insignificant or is of a smaller magnitude compared to the solar radiation impacts mediated via the ASM-ENSO teleconnection. These results suggest that minor changes in solar irradiance are likely amplified by changes in the ocean-atmosphere system related to ENSO teleconnections and, therefore, have a significant influence on ASM intensity. Modulation of solar irradiance on ENSO teleconnections has also been reported from other regions, such as North America (Li & Xiao, 2018; Osterberg et al., 2014), boreal polar regions (Kryjov & Park, 2007), and the Tibetan Plateau (Ming et al., 2020), suggesting that ENSO may act as a mediator between solar activity and its impact on terrestrial hydrology.

Additionally, this study reveals how TSI affects the ASM via modulating ENSO-ASM teleconnections on multi-decadal to centennial timescales. Previous work has mostly focused on changes in the mean state of ENSO and its consequent influence on ASM. For example, J. Zhang et al. (2021) proposed that the centennial-scale oscillations in EASM rainfall over the mid-YRV are closely related to increased rainfall corresponding to weakened solar irradiance and El Niño-like conditions. Our study emphasizes that changes in the strength and position of subtropical pressure systems in response to tropical SST anomalies play a critical role in the ENSO-EASM teleconnection. Furthermore, we found that the influence of the warm phase of ENSO on ASM is more sensitive to solar irradiance, a result also reported in previous studies focused on the ENSO teleconnection to North America (Li & Xiao, 2018).

The LM paleoclimate DA products (LMR and PHYDA) and climate model outputs (CESM-LME) explored in this work extend and complement previous studies based on either short-term instrumental observations (Mehta & Lau, 1997; Seetha et al., 2020) or sparse proxy records sensitive to the ASM systems (Neff et al., 2001; Sagawa et al., 2014; Tiwari et al., 2005; Y. Wang et al., 2005; J. Zhang et al., 2021). We acknowledge, however, that uncertainties and biases in climate models can impact the evolution of the ENSO-ASM relationship, as teleconnections in LMR and PHYDA are also largely defined by their model prior via covariance assumptions. For example, CESM-LME, which also provides the model prior to PHYDA, is known to overestimate the amplitude of ENSO compared with observations (Otto-Bliesner et al., 2016). Additionally, rainfall in the EASM region is overall positively correlated with Niño 3.4 in CESM, a simulated feature that opposes the relationship found in modern observations. However, owing to the lack of sufficient observational and paleoclimate validation information from East and South Asia, it is difficult to determine the role of model biases in our analysis. Moreover, there are key differences in the hydroclimate patterns between the three data sets. As mentioned above, PHYDA

uses CESM-LME (Otto-Bliesner et al., 2016) as its model prior with bias correction to the temperature and precipitation fields (Steiger et al., 2018), whereas LMR uses CCSM4 (Landrum et al., 2013) without bias correction (Hakim et al., 2016). Despite these large differences in the three data sets, their consistent responses in terms of the shift in the correlation coefficient between ASM and Niño 3.4 indices during periods of high and low TSI strongly support the assertion that the ASM-ENSO teleconnection is modulated by solar forcing.

The incorporation of additional hydroclimate-sensitive proxies from East and South Asia into DA products may afford large improvements to our ability to study the ENSO-ASM teleconnection. Though the physical teleconnections in DA products largely rely on model priors, paleoclimate proxies constrain the time evolution of reconstructions generated by the offline DA approach (Steiger et al., 2018), which is critically important for investigating the role of external forcing on the interannual ENSO-ASM relationship and its decadal variability. Future work should also explore the influence of solar forcing on ENSO-ASM teleconnections in different climate models, the physical mechanisms related to the asymmetric response of warm and cold ENSO events, and the role of the spatial pattern of SSTs over the tropical Pacific and Indian Ocean.

This work extends our understanding of how TSI impacts rainfall in the ASM region, with implications for decadal-scale hydroclimate prediction, and affords new avenues for testing models' response to natural external forcings with paleoclimate data. Anticipating the future hydroclimate response to global warming over broad swaths of Asia remains challenging due to uncertainties in the stability of the ENSO-ASM relationship. The ENSO-ASM teleconnection has undergone a significant shift since the 1970s (Chen et al., 2022; Kumar et al., 1999; Torrence & Webster, 1999; Wu & Wang, 2002), when anthropogenic radiative forcing due to greenhouse emissions increased more rapidly (IPCC, 2023). Moreover, the most recent sixth installment of the Coupled Model Intercomparison Project suggests over ∼50% of regions influenced by ENSO teleconnections are projected to experience significant changes in teleconnection rainfall under the highest emission scenarios (McGregor et al., 2022). Our study reveals that TSI is an important modulator of ENSO teleconnections to ASM regional rainfall via changes in tropical SST patterns and subtropical pressure systems.

Our findings from both paleoclimate DA products and numerical simulations imply that solar variability will compound with global warming to impact moisture supply over the densely populated ASM region. Whereas the evidence presented here suggests solar irradiance plays a role in modulating the ENSO-ASM teleconnection, its effect is likely to be strongly overpowered by anthropogenic GHG forcing; the radiative effect of GHG is an order of magnitude greater than that of changes in TSI (IPCC, 2023). Future research could compare the relative impacts of TSI and anthropogenic forcings (GHG, Aerosols) to fully assess how the impact of TSI will compound with radiative changes in the 21st century and alter the ENSO-ASM system, informing future projections of ASM rainfall.

Conflict of Interest

The authors declare no conflicts of interest relevant to this study.

Data Availability Statement

Last Millennium Reanalysis (LMR) Project Global Climate Reconstructions Version 2 is available at Tardif et al. (2019b). CESM-LME outputs can be downloaded from https://www.earthsystemgrid.org/dataset/ucar.cgd.ccsm4.cesmLME.html (Otto-Bliesner et al., 2016). Paleo Hydrodynamics Data Assimilation product (PHYDA) can be found at Steiger (2018). The GPCC monthly precipitation dataset can be downloaded from https://psl.noaa.gov/data/gridded/data.gpcc.html (Schneider et al., 2011).

Acknowledgments
X. D., S. D., and K. T. acknowledge funding from the National Science Foundation, P2C2 Grant 2102814, and K. T. additionally acknowledges funding from NSF via Award 2103077. J. H. acknowledges support from the Natural Science Foundation of Xiamen, China (Grant 3502Z20227019).

References

Agnihotri, R., Dutta, K., Bhushan, R., & Somayajulu, B. L. K. (2002). Evidence for solar forcing on the Indian monsoon during the last millennium. *Earth and Planetary Science Letters*, *198*(3), 521–527. https://doi.org/10.1016/S0012-821X(02)00530-7

Beer, J., Mende, W., & Stellmacher, R. (2000). The role of the sun in climate forcing. *Quaternary Science Reviews*, *19*(1), 403–415. https://doi.org/10.1016/S0277-3791(99)00072-4

Chang, C. P., Zhang, Y., & Li, T. (2000). Interannual and interdecadal variations of the East Asian summer monsoon and tropical Pacific SSTs. Part I: Roles of the subtropical ridge. *Journal of Climate*, *13*(24), 4310–4325. https://doi.org/10.1175/1520-0442(2000)013<4310:iaivot>2.0.co;2

Chen, L., Li, G., Long, S.-M., Gao, C., Zhang, Z., & Lu, B. (2022). Interdecadal change in the influence of El Niño in the developing stage on the central China summer precipitation. *Climate Dynamics*, *59*(5–6), 1265–1282. https://doi.org/10.1007/s00382-021-06036-9

Clift, P. D., & Plumb, R. A. (2008). *The Asian monsoon: Causes, history and effects* (Vol. 288). Cambridge University Press.
Emile-Geay, J., Cane, M., Seager, R., Kaplan, A., & Almasi, P. (2007). El Nino as a mediator of the solar influence on climate. *Paleoceanography*, *22*(3), PA3210. https://doi.org/10.1029/2006pa001304
Fan, K., Liu, Y., & Chen, H. (2012). Improving the prediction of the East Asian summer monsoon: New approaches. *Weather and Forecasting*, *27*(4), 1017–1030. https://doi.org/10.1175/WAF-D-11-00092.1
Goswami, B. (1998). Interannual variations of Indian summer monsoon in a GCM: External conditions versus internal feedbacks. *Journal of Climate*, *11*(4), 501–522. https://doi.org/10.1175/1520-0442(1998)011<0501:ivoism>2.0.co;2
Goswami, B. N., Krishnamurthy, V., & Annmalai, H. (1999). A broad-scale circulation index for the interannual variability of the Indian summer monsoon. *Quarterly Journal of the Royal Meteorological Society*, *125*(554), 611–633. https://doi.org/10.1002/qj.49712555412
Hakim, G. J., Emile-Geay, J., Steig, E. J., Noone, D., Anderson, D. M., Tardif, R., et al. (2016). The last millennium climate reanalysis project: Framework and first results. *Journal of Geophysical Research: Atmospheres*, *121*(12), 6745–6764. https://doi.org/10.1002/2016jd024751
Hu, J., Dee, S., Parajuli, G., & Thirumalai, K. (2023). Tropical Pacific modulation of the Asian summer monsoon over the last millennium in paleoclimate data assimilation reconstructions. *Journal of Geophysical Research: Atmospheres*, *128*(20), e2023JD039207. https://doi.org/10.1029/2023JD039207
Hu, Z. Z. (1997). Interdecadal variability of summer climate over East Asia and its association with 500 hPa height and global sea surface temperature. *Journal of Geophysical Research*, *102*(D16), 19403–19412. https://doi.org/10.1029/97jd01052
Huo, W., Xiao, Z., & Zhao, L. (2022). Phase-locked impact of the 11-year solar cycle on tropical Pacific decadal variability. *Journal of Climate*, *36*(2), 421–439. https://doi.org/10.1175/JCLI-D-21-0595.1
Huo, W., Xiao, Z., Zhao, L., & Liu, F. (2023). Ascending phase of solar cycle 25 tilts the current El Niño-Southern Oscillation transition. *Atmospheric and Oceanic Science Letters*, 100397. https://doi.org/10.1016/j.aosl.2023.100397
IPCC. (2023). Climate change 2023: Synthesis report. In Core Writing Team, H. Lee, & J. Romero (Eds.), *Contribution of Working Groups I, II and III to the Sixth Assessment Report of the Intergovernmental Panel on Climate Change* (pp. 35–115). IPCC. https://doi.org/10.59327/IPCC/AR6-9789291691647
Kalnay, E., Kanamitsu, M., Kistler, R., Collins, W., Deaven, D., Gandin, L., et al. (1996). The NCEP/NCAR 40-year reanalysis project. *Bulletin of the American Meteorological Society*, *77*(3), 437–472. https://doi.org/10.1175/1520-0477(1996)077<0437:TNYRP>2.0.CO;2
Krishnamurthy, V., & Goswami, B. N. (2000). Indian monsoon–ENSO relationship on interdecadal timescale. *Journal of Climate*, *13*(3), 579–595. https://doi.org/10.1175/1520-0442(2000)013<0579:IMEROI>2.0.CO;2
Kryjov, V. N., & Park, C.-K. (2007). Solar modulation of the El-Niño/Southern Oscillation impact on the Northern Hemisphere annular mode. *Geophysical Research Letters*, *34*(10), L10701. https://doi.org/10.1029/2006GL028015
Kumar, K. K., Rajagopalan, B., & Cane, M. A. (1999). On the weakening relationship between the Indian monsoon and ENSO. *Science*, *284*(5423), 2156–2159. https://doi.org/10.1126/science.284.5423.2156
Landrum, L., Otto-Bliesner, B. L., Wahl, E. R., Conley, A., Lawrence, P. J., Rosenbloom, N., & Teng, H. (2013). Last millennium climate and its variability in CCSM4. *Journal of Climate*, *26*(4), 1085–1111. https://doi.org/10.1175/JCLI-D-11-00326.1
Lau, K.-M., & Li, M.-T. (1984). The monsoon of East Asia and its global associations—A survey. *Bulletin of the American Meteorological Society*, *65*(2), 114–125. https://doi.org/10.1175/1520-0477(1984)065<0114:tmoeaa>2.0.co;2
Li, D., & Xiao, Z. (2018). Can solar cycle modulate the ENSO effect on the Pacific/North American pattern? *Journal of Atmospheric and Solar-Terrestrial Physics*, *167*, 30–38. https://doi.org/10.1016/j.jastp.2017.10.007
Lin, Y. F., Yu, J. Y., Wu, C. R., & Zheng, F. (2021). The footprint of the 11-year solar cycle in Northeastern Pacific SSTs and its influence on the Central Pacific El Niño. *Geophysical Research Letters*, *48*(5), e2020GL091369. https://doi.org/10.1029/2020gl091369
McGregor, S., Cassou, C., Kosaka, Y., & Phillips, A. S. (2022). Projected ENSO teleconnection changes in CMIP6. *Geophysical Research Letters*, *49*(11), e2021GL097511. https://doi.org/10.1029/2021GL097511
Meehl, G. A., Arblaster, J. M., Branstator, G., & van Loon, H. (2008). A coupled air–sea response mechanism to solar forcing in the Pacific region. *Journal of Climate*, *21*(12), 2883–2897. https://doi.org/10.1175/2007JCLI1776.1
Mehta, V. M., & Lau, K. M. (1997). Influence of solar irradiance on the Indian Monsoon-ENSO relationship at decadal-multidecadal time scales. *Geophysical Research Letters*, *24*(2), 159–162. https://doi.org/10.1029/96gl03778
Ming, G., Zhou, W., Cheng, P., Wang, H., Xian, F., Fu, Y., et al. (2020). Lacustrine record from the eastern Tibetan Plateau associated with Asian summer monsoon changes over the past ~ 6 ka and its links with solar and ENSO activity. *Climate Dynamics*, *55*(5), 1075–1086. https://doi.org/10.1007/s00382-020-05312-4
Misios, S., Gray, L. J., Knudsen, M. F., Karoff, C., Schmidt, H., & Haigh, J. D. (2019). Slowdown of the Walker circulation at solar cycle maximum. *Proceedings of the National Academy of Sciences*, *116*(15), 7186–7191. https://doi.org/10.1073/pnas.1815060116
Narasimha, R., & Bhattacharyya, S. (2010). A wavelet cross-spectral analysis of solar–ENSO–rainfall connections in the Indian monsoons. *Applied and Computational Harmonic Analysis*, *28*(3), 285–295. https://doi.org/10.1016/j.acha.2010.02.005
Neff, U., Burns, S. J., Mangini, A., Mudelsee, M., Fleitmann, D., & Matter, A. (2001). Strong coherence between solar variability and the monsoon in Oman between 9 and 6 kyr ago. *Nature*, *411*(6835), 290–293. https://doi.org/10.1038/35077048
Osterberg, E. C., Mayewski, P. A., Fisher, D. A., Kreutz, K. J., Maasch, K. A., Sneed, S. B., & Kelsey, E. (2014). Mount Logan ice core record of tropical and solar influences on Aleutian low variability: 500–1998 AD. *Journal of Geophysical Research: Atmospheres*, *119*(19), 11189–11204. https://doi.org/10.1002/2014jd021847
Otto-Bliesner, B. L., Brady, E. C., Fasullo, J., Jahn, A., Landrum, L., Stevenson, S., et al. (2016). Climate variability and change since 850 CE: An ensemble approach with the Community Earth System Model. *Bulletin of the American Meteorological Society*, *97*(5), 735–754. https://doi.org/10.1175/bams-d-14-00233.1
Palmer, T., Branković, Č., Viterbo, P., & Miller, M. (1992). Modeling interannual variations of summer monsoons. *Journal of Climate*, *5*(5), 399–417. https://doi.org/10.1175/1520-0442(1992)005<0399:mivosm>2.0.co;2
Park, J. Y., Jhun, J. G., Yim, S. Y., & Kim, W. M. (2010). Decadal changes in two types of the western North Pacific subtropical high in boreal summer associated with Asian summer monsoon/El Niño–Southern Oscillation connections. *Journal of Geophysical Research*, *115*(D21), D21129. https://doi.org/10.1029/2009jd013642
Rasmusson, E. M., & Carpenter, T. H. (1983). The relationship between eastern equatorial Pacific sea surface temperatures and rainfall over India and Sri Lanka. *Monthly Weather Review*, *111*(3), 517–528. https://doi.org/10.1175/1520-0493(1983)111<0517:TRBEEP>2.0.CO;2
Sagawa, T., Kuwae, M., Tsuruoka, K., Nakamura, Y., Ikehara, M., & Murayama, M. (2014). Solar forcing of centennial-scale East Asian winter monsoon variability in the mid-to late Holocene. *Earth and Planetary Science Letters*, *395*, 124–135. https://doi.org/10.1016/j.epsl.2014.03.043
Saha, A., Ghosh, S., Sahana, A. S., & Rao, E. P. (2014). Failure of CMIP5 climate models in simulating post-1950 decreasing trend of Indian monsoon. *Geophysical Research Letters*, *41*(20), 7323–7330. https://doi.org/10.1002/2014GL061573

Schneider, U., Becker, A., Finger, P., Meyer-Christoffer, A., Rudolf, B., & Ziese, M. (2011). GPCC full data reanalysis version 6.0 at 2.5°: Monthly land-surface precipitation from rain-gauges built on GTS-based and historic data [Dataset]. NOAA. https://doi.org/10.5676/DWD_GPCC/FD_M_V7_250

Seetha, C. J., Varikoden, H., Babu, C. A., & Kuttippurath, J. (2020). Significant changes in the ENSO-monsoon relationship and associated circulation features on multidecadal timescale. *Climate Dynamics*, *54*(3), 1491–1506. https://doi.org/10.1007/s00382-019-05071-x

Steiger, N. J. (2018). Paleo hydrodynamics data assimilation product (PHYDA) [Dataset]. Zenodo. https://doi.org/10.5281/zenodo.1198817

Steiger, N. J., Smerdon, J. E., Cook, E. R., & Cook, B. I. (2018). Data descriptor: A reconstruction of global hydroclimate and dynamical variables over the Common Era. *Scientific Data*, *5*(1), 180086. https://doi.org/10.1038/sdata.2018.86

Takahashi, H. G., & Fujinami, H. (2021). Recent decadal enhancement of Meiyu–Baiu heavy rainfall over East Asia. *Scientific Reports*, *11*(1), 1–8. https://doi.org/10.1038/s41598-021-93006-0

Tao, S.-Y. (1987). A review of recent research on the East Asian summer monsoon in China. *Monsoon meteorology*, 60–92.

Tardif, R., Hakim, G. J., Perkins, W. A., Horlick, K. A., Erb, M. P., Emile-Geay, J., et al. (2019a). Last Millennium Reanalysis with an expanded proxy database and seasonal proxy modeling. *Climate of the Past*, *15*(4), 1251–1273. https://doi.org/10.5194/cp-15-1251-2019

Tardif, R., Hakim, G. J., Perkins, W. A., Horlick, K. A., Erb, M. P., Emile-Geay, J., et al. (2019b). NOAA/WDS Paleoclimatology - Last Millennium Reanalysis (LMR) project global climate reconstructions version 2 [Dataset]. NOAA National Centers for Environmental Information. https://doi.org/10.25921/gn22-5866

Tiwari, M., Ramesh, R., Somayajulu, B. L. K., Jull, A. J. T., & Burr, G. S. (2005). Solar control of southwest monsoon on centennial timescales. *Current Science*, *89*(9), 1583–1588.

Torrence, C., & Webster, P. J. (1999). Interdecadal changes in the ENSO–monsoon system. *Journal of Climate*, *12*(8), 2679–2690. https://doi.org/10.1175/1520-0442(1999)012<2679:icitem>2.0.co;2

Trenberth, K. E. (1997). The definition of El Nino. *Bulletin of the American Meteorological Society*, *78*(12), 2771–2777. https://doi.org/10.1175/1520-0477(1997)078<2771:Tdoeno>2.0.Co;2

van Loon, H., Meehl, G. A., & Shea, D. J. (2007). Coupled air-sea response to solar forcing in the Pacific region during northern winter. *Journal of Geophysical Research*, *112*(D2), D02108. https://doi.org/10.1029/2006JD007378

Vieira, L. E. A., Solanki, S. K., Krivova, N. A., & Usoskin, I. (2011). Evolution of the solar irradiance during the Holocene. *Astronomy & Astrophysics*, *531*, A6. https://doi.org/10.1051/0004-6361/201015843

Wang, B., Gadgil, S., & Rupa Kumar, K. (2006). The Asian monsoon—Agriculture and economy. *The Asian Monsoon*, 651–683.

Wang, B., Wu, R., & Fu, X. (2000). Pacific–East Asian teleconnection: How does ENSO affect East Asian climate? *Journal of Climate*, *13*(9), 1517–1536. https://doi.org/10.1175/1520-0442(2000)013<1517:peathd>2.0.co;2

Wang, B., Wu, R., & Li, T. (2003). Atmosphere–warm ocean interaction and its impacts on Asian–Australian monsoon variation. *Journal of Climate*, *16*(8), 1195–1211. https://doi.org/10.1175/1520-0442(2003)16<1195:AOIAII>2.0.CO;2

Wang, B., Xiang, B., & Lee, J.-Y. (2013). Subtropical high predictability establishes a promising way for monsoon and tropical storm predictions. *Proceedings of the National Academy of Sciences*, *110*(8), 2718–2722. https://doi.org/10.1073/pnas.1214626110

Wang, J., & Zhao, L. (2012). Statistical tests for a correlation between decadal variation in June precipitation in China and sunspot number. *Journal of Geophysical Research*, *117*(D23), D23117. https://doi.org/10.1029/2012JD018074

Wang, J., Zhao, L., Xiao, Z., Zhang, P., Ren, Z., Zong, W., et al. (2023). Energy transmission processes in the effectuation chain of solar forcing to the terrestrial atmosphere—a review. *Frontiers in Earth Science*, *11*, 1164636. https://doi.org/10.3389/feart.2023.1164636

Wang, Y., Cheng, H., Edwards, R. L., He, Y., Kong, X., An, Z., et al. (2005). The Holocene Asian monsoon: Links to solar changes and North Atlantic climate. *Science*, *308*(5723), 854–857. https://doi.org/10.1126/science.1106296

Webster, P. J., Magana, V. O., Palmer, T. N., Shukla, J., Tomas, R. A., Yanai, M. U., & Yasunari, T. (1998). Monsoons: Processes, predictability, and the prospects for prediction. *Journal of Geophysical Research*, *103*(C7), 14451–14510. https://doi.org/10.1029/97jc02719

White, W. B., Lean, J., Cayan, D. R., & Dettinger, M. D. (1997). Response of global upper ocean temperature to changing solar irradiance. *Journal of Geophysical Research*, *102*(C2), 3255–3266. https://doi.org/10.1029/96jc03549

Wu, R., & Wang, B. (2002). A contrast of the East Asian summer monsoon–ENSO relationship between 1962–77 and 1978–93. *Journal of Climate*, *15*(22), 3266–3279. https://doi.org/10.1175/1520-0442(2002)015<3266:acotea>2.0.co;2

Yu, R., & Zhou, T. (2007). Seasonality and three-dimensional structure of interdecadal change in the East Asian monsoon. *Journal of Climate*, *20*(21), 5344–5355. https://doi.org/10.1175/2007JCLI1559.1

Zhang, J., Zhao, K., Wang, Y., Kong, X., Shao, X., Liang, Y., et al. (2021). Modulation of centennial-scale hydroclimate variations in the middle Yangtze River Valley by the East Asian-Pacific pattern and ENSO over the past two millennia. *Earth and Planetary Science Letters*, *576*, 117220. https://doi.org/10.1016/j.epsl.2021.117220

Zhang, R., Sumi, A., & Kimoto, M. (1996). Impact of El Niño on the East Asian monsoon a diagnostic study of the '86/87 and '91/92 events. *Journal of the Meteorological Society of Japan. Ser. II*, *74*(1), 49–62. https://doi.org/10.2151/jmsj1965.74.1_49

Zhao, L., & Wang, J. (2014). Robust response of the East Asian monsoon rainband to solar variability. *Journal of Climate*, *27*(8), 3043–3051. https://doi.org/10.1175/JCLI-D-13-00482.1

Zhao, L., Wang, J., Liu, H., & Xiao, Z. (2017). Amplification of solar signal in summer monsoon rainband in China by a synergistic action of different dynamical responses. *Journal of Meteorological Research*, *31*(1), 61–72. https://doi.org/10.1007/s13351-016-6046-6

Zhou, T., Yu, R., Zhang, J., Drange, H., Cassou, C., Deser, C., et al. (2009). Why the western Pacific subtropical high has extended westward since the late 1970s. *Journal of Climate*, *22*(8), 2199–2215. https://doi.org/10.1175/2008jcli2527.1

Zhou, T. J., & Yu, R. C. (2005). Atmospheric water vapor transport associated with typical anomalous summer rainfall patterns in China. *Journal of Geophysical Research*, *110*(D8), D08104. https://doi.org/10.1029/2004jd005413